The Astronomical Journal, 161:151 (7pp), 2021 March https://doi.org/10.3847/1538-3881/abdd2a

Reconstructing the Universe: Testing the Mutual Consistency of the Pantheon and SDSS/eBOSS BAO Data Sets with Gaussian Processes

Ryan E. Keeley[1], Arman Shafieloo[1,2], Gong-Bo Zhao[3,4], Jose Alberto Vazquez[5], and Hanwool Koo[1,2]
[1] Korea Astronomy and Space Science Institute, Daejeon 34055, Republic of Korea; rkeeley@kasi.re.kr
[2] University of Science and Technology, Daejeon 34113, Republic of Korea
[3] National Astronomy Observatories, Chinese Academy of Sciences, Beijing, 100012, People's Republic of China
[4] University of Chinese Academy of Sciences, Beijing 100049, People's Republic of China
[5] Instituto de Ciencias Fısicas, Universidad Nacional Autonoma de Mexico, Cuernavaca, Morelos, 62210, Mexico
Received 2020 October 27; revised 2021 January 14; accepted 2021 January 15; published 2021 February 25

Abstract

We test the mutual consistency between the baryon acoustic oscillation measurements from the eBOSS SDSS final release and the Pantheon supernova compilation in a model-independent fashion using Gaussian process regression. We also test their joint consistency with the ΛCDM model in a model-independent fashion. We also use Gaussian process regression to reconstruct the expansion history that is preferred by these two data sets. While this methodology finds no significant preference for model flexibility beyond ΛCDM, we are able to generate a number of reconstructed expansion histories that fit the data better than the best-fit ΛCDM model. These example expansion histories may point the way toward modifications to ΛCDM. We also constrain the parameters Ω_k and $H_0 r_d$ both with ΛCDM and with Gaussian process regression. We find that $H_0 r_d = 10{,}030 \pm 130$ km s^{-1} and $\Omega_k = 0.05 \pm 0.10$ for ΛCDM and that $H_0 r_d = 10{,}040 \pm 140$ km s^{-1} and $\Omega_k = 0.02 \pm 0.20$ for the Gaussian process case.

Unified Astronomy Thesaurus concepts: Cosmology (343); Baryon acoustic oscillations (138); Redshift surveys (1378); Dark energy (351); Type Ia supernovae (1728); Astrostatistics techniques (1886)

1. Introduction

ΛCDM (Λ for a cosmological constant and CDM for cold dark matter) has emerged as the concordance model of cosmology. This model explains a number of data sets well, at least individually. In broad strokes, the ΛCDM model explains well the anisotropies in the cosmic microwave background, how those anisotropies cluster and grow into the observed large-scale structure of the universe, and how the expansion of the universe accelerates at late times.

However, there have emerged a number of tensions in the ΛCDM parameters inferred by different data sets. Most notably is the so-called "H_0 tension," which is a 4.4σ discrepancy between the present-day expansion rate directly observed from the Cepheid anchoring of supernova distances (SN; Riess et al. 2019) and that rate inferred from Planck measurements of the cosmic microwave background (Planck Collaboration et al. 2020). Other low-redshift distances, including strong lens time delay distances (Liao et al. 2020; Wong et al. 2020) and the Tip of the Red Giant Branch (Freedman et al. 2020) measurements also show some tension, though these are less precise. There are a number of other tensions involving the growth of structure (Hildebrandt et al. 2017; Heymans et al. 2020) and the inferred curvature (Handley 2021; Di Valentino et al. 2020). Taken together, these may point toward a discrepancy between high- and low-redshift physics (Keeley et al. 2019).

The H_0 tension is primarily about the absolute scale of the distance–redshift relation, but the shape of this relation can point toward a possible extension to ΛCDM that may explain the H_0 tension. Two tracers of the shape of the distance–redshift relation are SN distances and the baryon acoustic oscillations (BAO) feature in the clustering of galaxies. Jointly, the SN and BAO data sets are particularly relevant for this H_0 tension because they are anchored by the two data sets in question (Cepheids and the CMB). Indeed, if the H_0 measurement from the Cepheids is taken to anchor the SN and r_d, the size of the sound horizon at the drag epoch, is taken to anchor the BAO, then the distances inferred from the two data sets are discrepant regardless of any cosmological interpretation of those distances (Knox & Millea 2020). Thus, the two data sets, even on their own and unanchored, can indicate what new physics might be needed to explain the H_0 tension.

While there have emerged a large number of explanations that have reconciled the Planck "TT" data set and the Cepheid data set, most have not been able to jointly explain every cosmological data set. Notably, modifying the physics at high redshift can alleviate the tension between the temperature data set and the SH0ES data set, though since the posterior does not shift much, but just expands, adding in the polarization data sets causes tension to reemerge (Bernal et al. 2016; Agrawal et al. 2019; Poulin et al. 2019; Hill et al. 2020). Similarly, low-redshift modifications tend to have trouble simultaneously explaining both the BAO and SN distances (Keeley et al. 2019; Li & Shafieloo 2019, 2020). Rather than iterate through a possibly infinite number of nested extensions to ΛCDM or discrete alternative models, it can be more fruitful to use model-independent methods. That is, it is better to use data-driven techniques to reconstruct the distance–redshift relation from the data directly. With the reconstructions, one can then build a model around what is revealed by the data.

In this paper, we first (Section 2) seek to use model-independent methods to test that the SN and BAO distances are, in fact, consistent with each other and that they are jointly consistent with the ΛCDM model. In Section 3, we then reconstruct the expansion history of the universe ($h(z)$) inferred from these two data sets, as well as additional diagnostics that test the consistency with ΛCDM ($om(z)$ and $q(z)$). We continue in Section 4 where we use our model-independent methods to constrain the relative anchoring of the two SN and BAO

distance data sets ($H_0 r_d$) as well as constrain the curvature (Ω_k). We compare the model-independent results with those inferred by ΛCDM. We discuss these results and conclude in Section 5.

2. Consistency Tests

In this section, we use Gaussian process (GP) regression to perform model-independent tests of the mutual consistency of the Pantheon (Scolnic et al. 2018) and SDSS (Blanton et al. 2017) eBOSS (Dawson et al. 2016; eBOSS Collaboration et al. 2020) BAO data sets and their joint consistency with the ΛCDM model. It is important to perform consistency tests to answer whether there are any systematics that might hinder the ability to interpret these distances accurately. Further, if the data sets have some certain systematic between them, any attempt to derive cosmological parameters from a joint inference of the two data sets will yield inaccurate and artificially precise results. The inferred posteriors would be meaningless. Additionally, it is important to perform these kinds of tests in a model-independent manner so that we can avoid making assumptions that we would want to test, thus making any outcome of the test more robust.

Previous tests of the consistency between SN and BAO have relied on model assumptions. The most recent of such tests is found in the eBOSS cosmology interpretation paper (eBOSS Collaboration et al. 2020). This test calculates the posterior of the individual data sets and see if they overlap. They found that the posteriors overlap in the curved-ΛCDM parameter space, though the conclusion that the data sets are consistent is necessarily contingent on the assumed model. If additional extensions to ΛCDM were used, then it is conceivable the posteriors would no longer overlap. Our model-independent method tests the consistency for a large class of expansion histories and thus relaxes the assumption of the model and makes the conclusions more robust.

2.1. Data Sets

Both the Pantheon (Scolnic et al. 2018) and SDSS BAO (eBOSS Collaboration et al. 2020) data sets are unanchored, so it is trivial to get the absolute scale of the data sets to agree. Therefore, we are effectively only testing if the shapes of the inferred expansion histories are consistent. In other words, these two data sets, on their own, will not be able to adjudicate which value of H_0 is correct, but they will be able to adjudicate the kinds of beyond-ΛCDM modifications can explain the tension. If the two data sets are consistent with each other and with ΛCDM, then we can be more sure that the modification must occur outside the redshift range of the data sets. One possible interpretation of any inconsistency that might be found is that the cosmic distance duality relation is violated, that the angular diameter distances ($D_A(z)$) and the luminosity distances ($D_L(z)$) are related by $(1+z)^2 D_A(z)/D_L(z) = 1$ (Liao 2019).

The Pantheon SN data set is composed of 1048 Type Ia SN between $z = 0.01$ and $z = 2.3$. SN are able to constrain cosmological distances because they are empirically assumed to be standardizable candles. That is, SN with the same lightcurves, modulo the color and stretch of the SN and properties of the host galaxy, are thought to have the same intrinsic luminosity. This intrinsic luminosity, parameterized by M_b, is unknown, however, and degenerate with H_0. Therefore, measuring the brightnesses of SN can yield information about the relative distances of the SN but not their absolute distances. SN constrain the shape of the expansion history but they are unanchored.

The SDSS BAO data set measures the correlation function of galaxies. This correlation function contains a "BAO feature" that is an overdensity of power at the drag scale r_d. This feature arises from sound waves in the plasma of the early universe. This scale is fixed in comoving units and is encoded in the clustering of galaxies.

The SDSS eBOSS final release measures the BAO feature in a variety of tracers over a variety of redshifts, with the Main Galaxy Sample at $z = 0.15$ (Howlett et al. 2015; Ross et al. 2015), the BOSS Luminous Red Galaxy sample at redshifts $z = 0.38$ and 0.51 (Alam et al. 2017; Beutler et al. 2017; the $z = 0.61$ bin from this sample is merged into the eBOSS sample), the eBOSS Luminous Red Galaxy sample at redshift $z = 0.70$ (eBOSS Collaboration et al. 2020), the eBOSS Emission-line Galaxy sample at redshift $z = 0.85$ (eBOSS Collaboration et al. 2020), the eBOSS quasar sample at redshift $z = 1.48$ (eBOSS Collaboration et al. 2020), and the BOSS/eBOSS Lyα forest and quasar sample at $z = 2.33$ (du Mas des Bourboux et al. 2017, 2020). We use the full likelihoods of the SDSS/eBOSS collaboration.[6]

2.2. Gaussian Process

A GP is an infinite collection of correlated random variables characterized by a covariance function (Rasmussen & Williams 2006). Where a Gaussian distribution draws a single number, a GP generalizes this concept and draws a function. So, in a sense, GP can be thought of as a sampling method, but instead of sampling over a finite dimensional parameter space as in Markov chain Monte Carlo (MCMC), GP samples an infinite dimensional function space.

GP generally can take an input called a mean function, a function about which the random fluctuations of the GP varies. Therefore, the draws of a GP can be thought of as hyperfunctions (not the holomorphic variety, just a generalization of a hyperparameter, i.e., a function to be marginalized over), and therefore GP can be used as a method to look for deviations away from this mean function. To test ΛCDM, we can choose it as the mean function for our GP inferences.

Using GP to perform a regression utilizes both these understandings of GP. We essentially take a GP as the prior in a Bayesian analysis. In proper Bayesian fashion, we marginalize over this family of hyperfunctions drawn from the GP prior. Each of these hyperfunction samples is weighted by their likelihood, by how well they fit the data. Histogramming each of these weighted hyperfunctions then allows us to calculate the posterior, not in terms of a set of parameters, but directly in terms of the reconstructed cosmological functions, for instance, the expansion history $H(z)$. We can summarize the methodology up to this point with the equation via Bayes' theorem,

$$P(H(z)|D) = \int d\phi_{\rm GP}\, \mathcal{L}(D|H(z, \phi_{\rm GP}))P(\phi_{\rm GP})/P(D), \quad (1)$$

where $\phi_{\rm GP}$ is the family of hyperfunctions from the GP, D is the data, $P(H(z)|D)$ is the posterior, $\mathcal{L}(D|H(z, \phi_{\rm GP}))$ is the likelihood, $P(\phi_{\rm GP})$ is the prior, and $P(D)$ is the evidence. The hyperfunctions are related to the expansion history by the

[6] https://svn.sdss.org/public/data/eboss/DR16cosmo/tags/v1_0_0/likelihoods/

following formula,

$$H(z) = H_{mf}(z)\exp(\phi(z)), \tag{2}$$

where $H_{mf}(z)$ is the expansion history of the mean function. From the posterior, we can calculate quantities like the 68% and 95% confidence levels (CL) for the value of $H(z)$ at any particular redshift. Joining the CLs for various redshifts allows us to generate the "band" plots, which if the data significantly prefer some amount of evolution in the expansion history, relative to the mean function, then it will show up in these plots.

As mentioned previously, a GP is characterized by a covariance function. This covariance function can be quite general so long as it satisfies some general properties like being symmetric and positive semidefinite. We specifically use a squared-exponential covariance matrix with the following form,

$$\langle \phi(s_1)\phi(s_2)\rangle = \sigma_f^2\, e^{-(s_1-s_2)^2/(2\ell^2)}, \tag{3}$$

where our evolution variable is $s(z) = \log(1+z)/\log(1+z_{\max})$. We take $z_{\max} = 3$. Importantly, the covariance function is characterized by two hyperparameters. Parameter σ_f determines the heights of the random fluctuations of the GP, i.e., the scale of the deviations away from the mean function. If the data prefer additional information or flexibility beyond the input mean function, they will pick out a value for σ_f above zero. Parameter ℓ determines the length of the random fluctuations. In simple terms, $1/\ell$ is roughly the number of independent random fluctuations in the range. So GP samples with large ℓ and large σ_f would have a few large deviations, while small ℓ and small σ_f would have many smaller deviations. Because these hyperparameters encode information about the inferred expansion histories, the hyperparameters must be fit for and cannot be assumed.

One might be concerned that this sort of analysis is prone to overfitting. If ℓ is small, say $\ell \sim 0.001$, that is, in effect, $\sim$1000 degrees of freedom and the worry is that this analysis could easily achieve an arbitrarily good χ^2 value. It is possible for GP to generate a sample that has this feature, however, for a GP with $\ell \sim 0.001$, the variety of functions that it can produce is vast and so it would be rare for the GP to actually generate this hypothetical example. In other words, because we marginalize over the space of possible functions, we avoid overfitting. Bayesian analyses are typically safe from the overfitting problem.

It is these hyperparameters that can be used for testing whether the data are consistent with the mean function of the GP regression (Shafieloo et al. 2012, 2013; Aghamousa et al. 2017; L'Huillier et al. 2019; Keeley et al. 2020). Since σ_f determines the size of the deviations away from the mean function, the test of the consistency of the mean function with the data amounts to testing if σ_f is consistent with 0. So in effect, we calculate the posterior for the hyperparameters σ_f and ℓ and see where CLs end up. This GP code is based in `gphist` (Kirkby & Keeley 2017), which is first introduced in Joudaki et al. (2018) and later refined in Keeley et al. (2019, 2020). We use scale invariant priors for σ_f and ℓ.

2.3. Testing ΛCDM

Now that we have a general methodology to test whether the mean function of a GP is consistent with the data, we can test if the two data sets are jointly consistent with the ΛCDM model. This is achieved simply by fitting ΛCDM to the two data sets, finding which parameters fit them best, and then using the expansion history of this best-fit ΛCDM model as the mean function. Thus if the posterior of σ_f is consistent with 0, then ΛCDM is consistent with the two data sets jointly. We see the results of this test in the bottom panel of Figure 1. There the posterior is shown with the color corresponding to $-\log(P(\sigma_f, \ell|D))$ and the 68%, 95%, and 99.7% CLs. We see that $\sigma_f = 0$ and therefore ΛCDM is consistent with the two data sets.

2.4. Testing Mutual Consistency

In order to test the mutual consistency of the two data sets we can choose the mean function to be a GP reconstruction of one of the data sets to serve as the mean function for a GP reconstruction of the other. Schematically, we start with the best-fit ΛCDM expansion history to the SDSS BAO data set, for example, which we use as a mean function for a GP regression of that same data set. We then use the median GP reconstruction of the SDSS BAO data set as a mean function for a GP regression of the Pantheon data set. The posterior of the hyperparameters for this second GP regression is what is shown in the upper panels of Figure 1. The top-left panel of that figure corresponds the GP regression of the SDSS BAO data set with a GP reconstruction from the Pantheon data set as a mean function. The top-right panel is the reverse, a GP regression of the Pantheon data set with a mean function taken from the GP reconstruction from the SDSS BAO data set. In both cases, we see that the posteriors of the hyperparameters are consistent with $\sigma_f = 0$ and therefore the data prefer no additional information beyond the mean function. The distances inferred from the SDSS BOSS and Pantheon data sets are consistent.

3. Reconstructions

In this section, we present reconstructions of various parameters of the universe's expansion history that are independent of the absolute scale of the expansion history, including $h(z) = H(z)/H_0$, the deceleration parameter $q(z)$, and the om diagnostic $om(z)$; (Sahni et al. 2008). The deceleration parameter is given by the following formula,

$$q(z) = -\frac{\ddot{a}a}{\dot{a}^2} = -1 + \frac{d\log H(z)}{d\log(1+z)}, \tag{4}$$

and the om diagnostic is given by

$$om(z) = \frac{h(z)^2 - 1}{(1+z)^3 - 1}. \tag{5}$$

Each of these parameters are potentially useful for testing whether the GP reconstructions are consistent with ΛCDM or if some evolution is preferred. The dimensionless expansion history, $h(z)$, is the most obvious and direct quantity to reconstruct from the data, however, its interpretation is more uncertain because the variation within ΛCDM can look categorically similar to the variation within models of evolving dark energy. Specific functions of $h(z)$, however, can make more robust tests of ΛCDM or not ΛCDM.

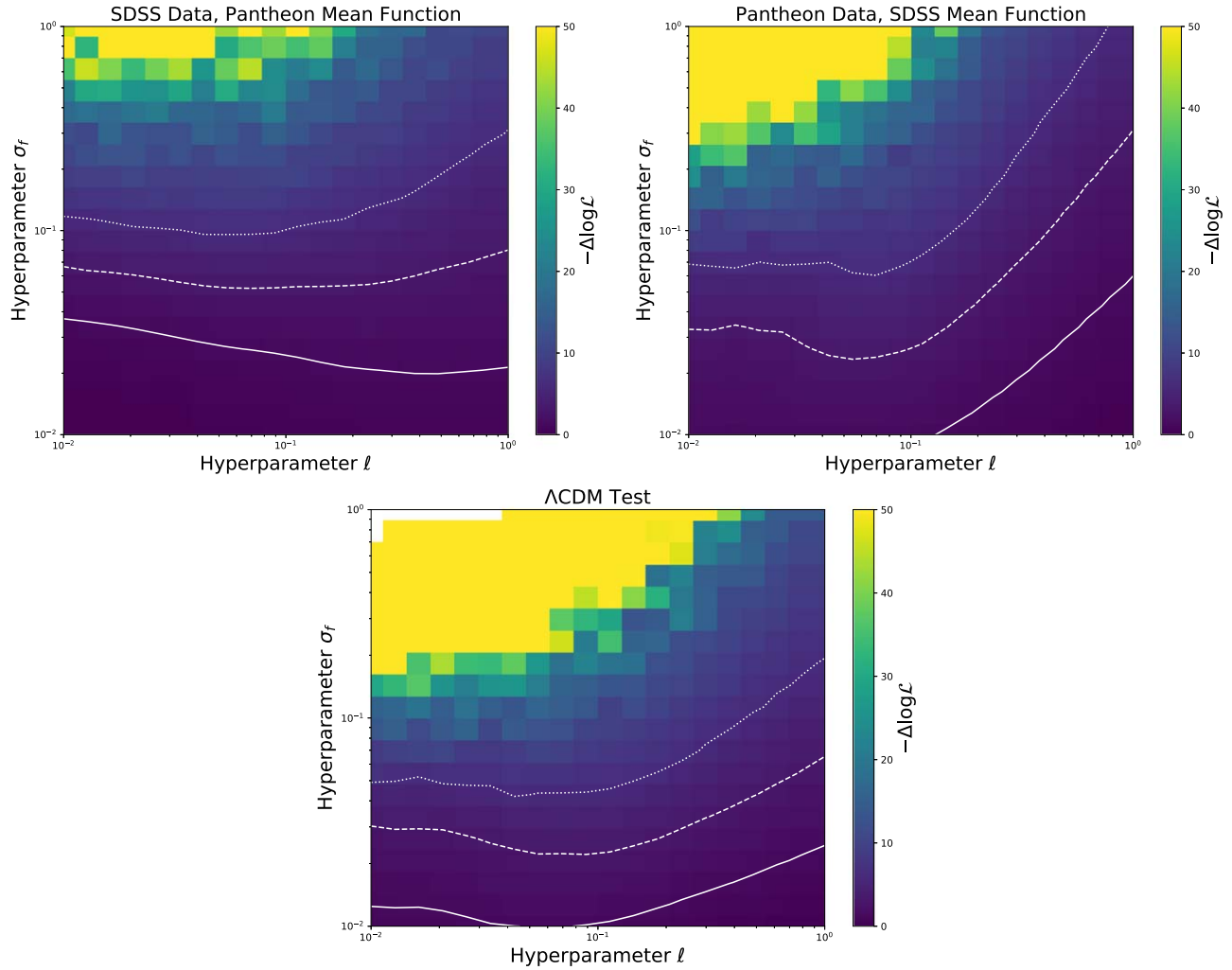

Figure 1. Hyperparameter posteriors for three different cases of consistency checks. The solid, dashed, and dotted white lines correspond to the 1σ, 2σ, and 3σ contours of the posterior, respectively. The top-left case corresponds to a GP inference of the SDSS data with a mean function taken from a best-fit GP sample to the SN data; the top-right is the same but switched: a GP inference of SN data with a mean function taken from a best-fit GP sample to the SDSS data. The bottom case corresponds to a GP inference of both the SN and SDSS data with a mean function taken from the best-fit ΛCDM fit to the two data sets.

For instance, $om(z)$ should be constant and equal to the matter density $\Omega_{\rm m}$ if ΛCDM correctly described the low-redshift distances. Any evolution in the expansion history, for example from an evolving dark energy, would show up as an evolution in this parameter. Since this parameter has divided out the ΛCDM evolution from $h(z)$, any potential beyond-ΛCDM evolution will be more prominent in this function than in $h(z)$.

Similarly, for ΛCDM $1 + q(z) = \frac{3}{2}\frac{\Omega_m(1+z)^3}{\Omega_{\rm crit}(z)}$, so at high redshifts it is equal to $3/2$ and then transitions to $3/2\,\Omega_m$ by $z = 0$. Since this parameter is, effectively, the second derivative of the data, using a model-independent method to constrain this quantity will necessarily give uncertain and noisy results.

The results of these reconstructions are shown in Figure 2. The lighter blue shaded regions correspond to the 68% and 95% CLs of the GP regression. These quantities are calculated by taking each GP reconstruction, calculating $h(z)$, $om(z)$, and $q(z)$ for each, then, for each redshift, grabbing the quantity at that redshift, and then making a histogram over all of the different reconstructions, weighted by their likelihoods. We use these histograms to calculate the 68% and 95% CLs.

In orange, we show the corresponding CLs, but for the case where ΛCDM is assumed. The notable feature here is that the ΛCDM case yields tighter constraints on these functions of the expansion history. This feature is expected, since, by construction, the GP case is more agnostic about the expansion history.

On top of these bands, we plot specific GP reconstructions that have a better χ^2 than the best-fit ΛCDM. The reconstructions of $om(z)$ have some noticeable, though rare, evolution toward low redshift, though this is the region where this quantity is least constrained by the data.

From these reconstructions, we can see that the Pantheon and SDSS BAO data sets prefer no significant evolution with respect to ΛCDM model and show a nonexhaustive set of example expansion histories that happen to fit these data sets better then the best-fit ΛCDM.

However, there do exist a number of GP reconstructions that fit the data better than the best-fit ΛCDM model (see Table 1). An examination of the GP hyperparameters that generated these reconstructions can give insight into what features of the data the reconstructions are fitting better than ΛCDM. Most of these better-than-ΛCDM reconstructions have large ℓ values

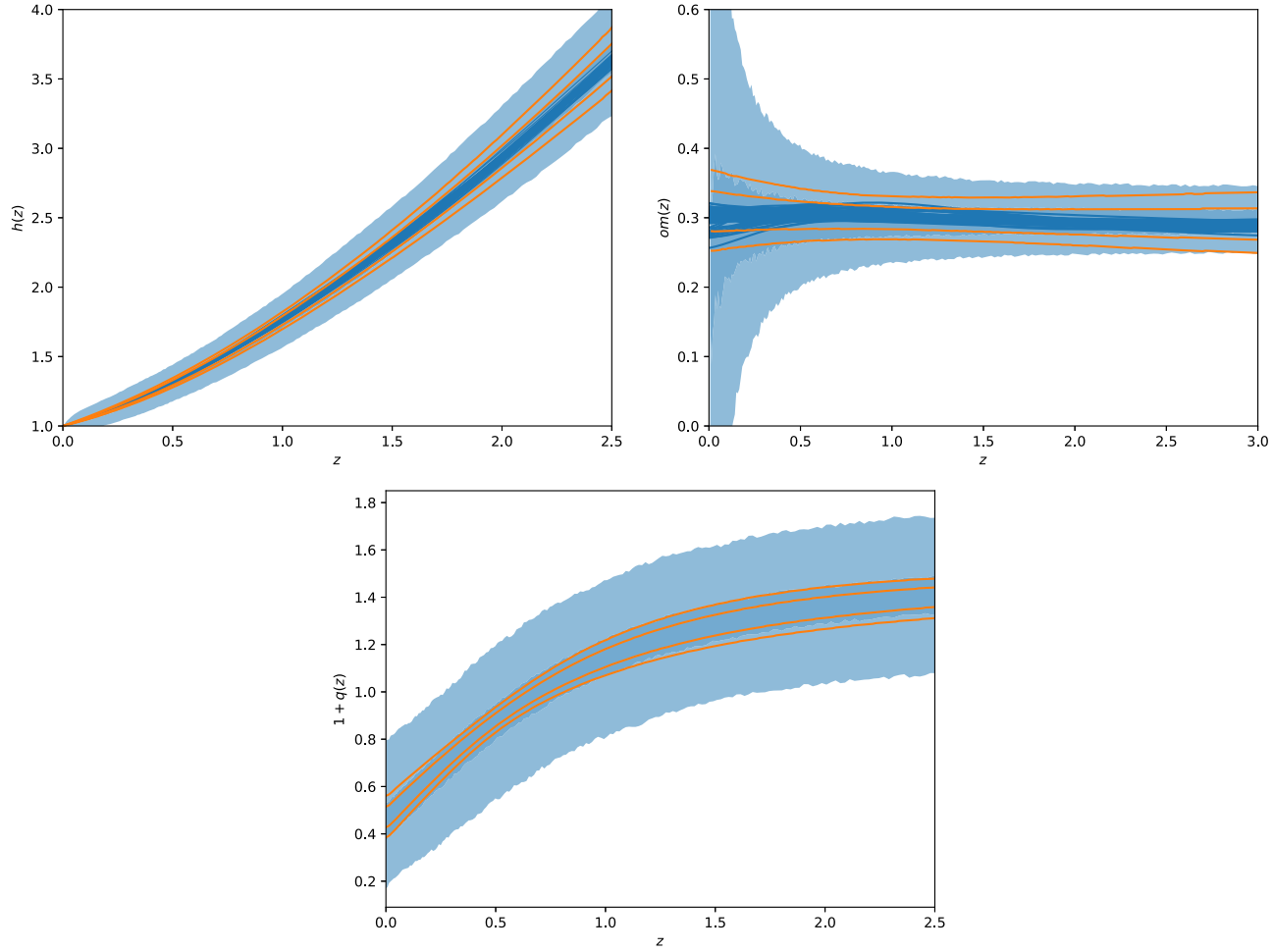

Figure 2. GP reconstructions of $h(z)$, $q(z)$, and $om(z)$. The blue bands represent the 68% and 95% confidence levels for the GP reconstructions and the darkest blue lines represent example GP samples that fit the data better than the best-fit ΛCDM model. The orange lines enclose the 68% and 95% confidence levels for the ΛCDM case.

Table 1
Best-fit χ^2 Values for the ΛCDM and GP Cases

	SN	SDSS	SN+SDSS
ΛCDM	1027	7	1034
GP	1023	5	1028

while only having a better fit by $\Delta\chi^2 \sim 0.1-1.0$. The GP reconstructions that have the best fit to the data ($\Delta\chi^2 = 6$) also have the smallest values of ℓ, which, in some sense, translates to a large number of degrees of freedom, so these reconstructions have rapidly varying $h(z)$. They vary in such a way that $h(z)$ is not monotonically increasing with redshift, indicating for that reconstruction that the inferred dark energy density would have to be negative at some point. It might be reasonable to reject any reconstruction that would have a negative dark energy density at any point on purely a priori grounds, but it is still interesting to see what sort of expansion history is needed to fit the data better than ΛCDM. Taken together, each of these discussed features point toward the conclusion that these reconstructions that fit the data better than ΛCDM are merely overfitting the noise in the data.

4. Anchors and Curvature

In this section, we use the SDSS BAO measurements alongside the Pantheon SN distances to constrain $H_0 r_d$. This parameter is the relative anchor of these two unanchored data sets. The SN constrain unanchored distances, or similarly, they constrain $h(z) = H(z)/H_0$. The individual BAO constraints measure $H(z)r_d$ or D_M/r_d at various redshifts. However, to get $H_0 r_d$, one still needs to make assumptions to project down to $z = 0$. This is where the SN enter, since it is in this region that they have the greatest constraining power. Therefore, combining the two data sets can yield robust and tight constraints on $H_0 r_d$, even with model-independent methods.

It is trivial to calculate this in the ΛCDM case. The low-redshift expansion history and distances are simply given by the typical parameters H_0, Ω_m, and Ω_k. We also fit for M_b and r_d to calibrate the distances from the Pantheon and SDSS BAO data sets. Where normally, within ΛCDM, r_d is a derived parameter that depends on the other parameters of the background model (e.g., any extra radiation before recombination could affect r_d), in this analysis, because we are only fitting low-redshift distances, we seek to remain agnostic about any potential beyond-ΛCDM modifications that might affect r_d. Therefore, we treat r_d as an independent parameter and fit for it

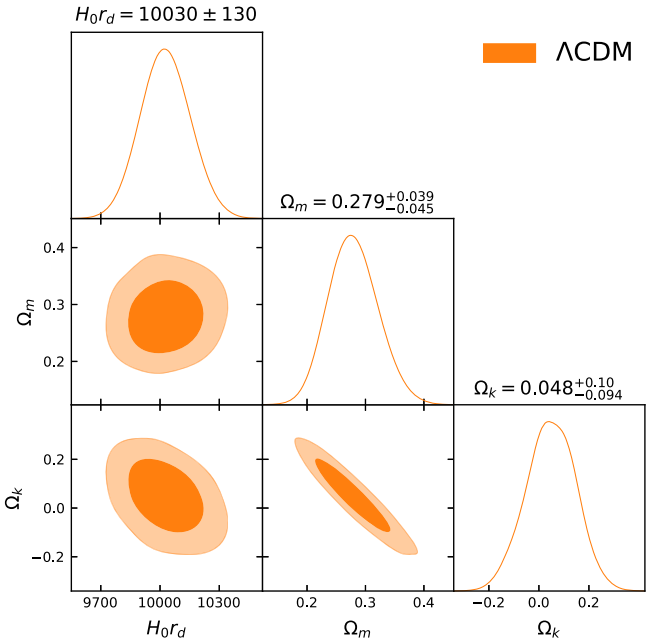

Figure 3. Posteriors of the ΛCDM parameters.

independently of the other parameters. In summary, we vary the five mentioned parameters (H_0, Ω_m, Ω_k, M_b, and r_d) and use MCMC to calculate the posterior of these parameters. Thus, it is relatively trivial to express the constraint in terms of $H_0 r_d$; the samples of $H_0 r_d$ are simply the multiplication of the samples of H_0 and r_d.

Each sample from the GP is a randomly generated $H(z)$, so H_0 in this case is simply $H(z=0)$. For the GP case, we also treat M_b and r_d as nuisance parameters, so we also fit for these parameters alongside the expansion histories generated from the GP. Thus, again, the samples of $H_0 r_d$ are simply the multiplication of the samples of $H(z=0)$ and r_d. Since the BAO data set constrains both the angular diameter distances $D_M(z)$ and the expansion rate $H(z)$, the GP can constrain the curvature, since

$$D_M(z) = \Omega_k^{-1/2} \sinh\left[\Omega_k^{1/2} c \int_0^z dz'/H(z')\right]. \quad (6)$$

The GP case cannot constrain the matter density in a similar way since for any Ω_m, one can then choose $w(z)$ to get the $H(z)$ needed for the GP reconstruction.

As seen in Figure 3 for the ΛCDM case, we find that $H_0 r_d = 10{,}030 \pm 130$ km s^{-1}, $\Omega_m = 0.28 \pm 0.04$, and $\Omega_k = 0.05 \pm 0.10$, and for the GP case, we find that that $H_0 r_d = 10{,}040 \pm 140$ km s^{-1} and $\Omega_k = 0.02 \pm 0.20$.

5. Discussion and Conclusions

These results can be used to constrain the low-redshift expansion history and so SN and BAO can adjudicate low-redshift explanations for the H_0 tension, e.g., curvature or evolving dark energy.

These results can also be used to constrain any potential evolution of the SN. It has been claimed (Kim et al. 2019) that SN might not show any evidence for an accelerating universe or for dark energy. The claim instead is that SN evolve with redshift, that either the lightcurve calibration with SALT-2 or the Tripp formula would need extra freedom to account for properties of the host galaxy. Our methodology implicitly constrains these ideas. Since we found that both the reconstructed expansion histories from the SN and from the BAO are consistent with each other and with ΛCDM, any astrophysical evolution would break this consistency and thus be disfavored.

This shows that the inference of dark energy is dependent on not just the SN data set; the BAO data set confirms this as well.

In this paper, we use GP regression to show that the SN and BAO data sets are consistent with each other and with ΛCDM. Further, we reconstruct dimensionless functions of the expansion history of the universe, $h(z)$, $q(z)$, $om(z)$. This allows us to visually inspect the consistency between these data sets and the ΛCDM model and to demonstrate that there is still some flexibility allowed at low redshifts. Finally, we calculate ΛCDM posteriors from the two data sets finding that $H_0 r_d = 10{,}030 \pm 130$ km s^{-1}, $\Omega_m = 0.28 \pm 0.04$, and $\Omega_k = 0.05 \pm 0.10$. We also constrain $H_0 r_d$ and Ω_k using our nonparametric GP method, finding that $H_0 r_d = 10{,}040 \pm 140$ km s^{-1} and $\Omega_k = 0.02 \pm 0.20$.

This work was supported by the high-performance computing clusters Seondeok at the Korea Astronomy and Space Science Institute. A. S. would like to acknowledge the support of the Korea Institute for Advanced Study (KIAS) grant funded by the government of Korea. G.B.Z. is supported by the National Key Basic Research and Development Program of China (No. 2018YFA0404503), a grant of CAS Interdisciplinary Innovation Team, and NSFC Grants 11925303, 11720101004, 11673025 and 11890691.

Funding for the Sloan Digital Sky Survey IV has been provided by the Alfred P. Sloan Foundation, the U.S. Department of Energy Office of Science, and the Participating Institutions. SDSS acknowledges support and resources from the Center for High-Performance Computing at the University of Utah. The SDSS website is www.sdss.org.

SDSS is managed by the Astrophysical Research Consortium for the Participating Institutions of the SDSS Collaboration including the Brazilian Participation Group, the Carnegie Institution for Science, Carnegie Mellon University, Center for Astrophysics Harvard & Smithsonian (CfA), the Chilean Participation Group, the French Participation Group, Instituto de Astrofísica de Canarias, The Johns Hopkins University, Kavli Institute for the Physics and Mathematics of the Universe (IPMU)/University of Tokyo, the Korean Participation Group, Lawrence Berkeley National Laboratory, Leibniz Institut für Astrophysik Potsdam (AIP), Max-Planck-Institut für Astronomie (MPIA Heidelberg), Max-Planck-Institut für Astrophysik (MPA Garching), Max-Planck-Institut für Extraterrestrische Physik (MPE), National Astronomical Observatories of China, New Mexico State University, New York University, University of Notre Dame, Observatório Nacional/MCTI, The Ohio State University, Pennsylvania State University, Shanghai Astronomical Observatory, United Kingdom Participation Group, Universidad Nacional Autónoma de México, University of Arizona, University of Colorado Boulder, University of Oxford, University of Portsmouth, University of Utah, University of Virginia, University of Washington, University of Wisconsin, Vanderbilt University, and Yale University.

ORCID iDs

Ryan E. Keeley https://orcid.org/0000-0002-0862-8789
Arman Shafieloo https://orcid.org/0000-0001-6815-0337
Gong-Bo Zhao https://orcid.org/0000-0003-4726-6714
Hanwool Koo https://orcid.org/0000-0003-0268-4488

References

Aghamousa, A., Hamann, J., & Shafieloo, A. 2017, JCAP, 2017, 031
Agrawal, P., Cyr-Racine, F.-Y., Pinner, D., & Randall, L. 2019, arXiv:1904.01016
Alam, S., Ata, M., Bailey, S., et al. 2017, MNRAS, 470, 2617
Bernal, J. L., Verde, L., & Riess, A. G. 2016, JCAP, 2016, 019
Beutler, F., Seo, H.-J., Ross, A. J., et al. 2017, MNRAS, 464, 3409
Blanton, M. R., Bershady, M. A., Abolfathi, B., et al. 2017, AJ, 154, 28
Dawson, K. S., Kneib, J.-P., Percival, W. J., et al. 2016, AJ, 151, 44
Di Valentino, E., Melchiorri, A., & Silk, J. 2020, NatAs, 4, 196
du Mas des Bourboux, H., Le Goff, J.-M., Blomqvist, M., et al. 2017, A&A, 608, A130
du Mas des Bourboux, H., Rich, J., Font-Ribera, A., et al. 2020, ApJ, 901, 153
eBOSS Collaboration, Alam, S., Aubert, M., et al. 2020, arXiv:2007.08991
Freedman, W. L., Madore, B. F., Hoyt, T., et al. 2020, ApJ, 891, 57
Handley, W. 2021, PhRvD, 103, L041301
Heymans, C., Tröster, T., Asgari, M., et al. 2020, arXiv:2007.15632
Hildebrandt, H., Viola, M., Heymans, C., et al. 2017, MNRAS, 465, 1454
Hill, J. C., McDonough, E., Toomey, M. W., & Alexander, S. 2020, PhRvD, 102, 043507
Howlett, C., Ross, A. J., Samushia, L., Percival, W. J., & Manera, M. 2015, MNRAS, 449, 848
Joudaki, S., Kaplinghat, M., Keeley, R. E., & Kirkby, D. 2018, PhRvD, 97, 123501
Keeley, R. E., Joudaki, S., Kaplinghat, M., & Kirkby, D. 2019, JCAP, 2019, 035
Keeley, R. E., Shafieloo, A., L'Huillier, B., & Linder, E. V. 2020, MNRAS, 491, 3983
Kim, Y.-L., Kang, Y., & Lee, Y.-W. 2019, JKAS, 52, 181
Kirkby, D., & Keeley, R. E. 2017, Cosmological Expansion History Inference Using Gaussian Processes, v1.0, Zenodo, doi:10.5281/zenodo.999564
Knox, L., & Millea, M. 2020, PhRvD, 101, 043533
L'Huillier, B., Shafieloo, A., Linder, E. V., & Kim, A. G. 2019, MNRAS, 485, 2783
Li, X., & Shafieloo, A. 2019, ApJL, 883, L3
Li, X., & Shafieloo, A. 2020, ApJ, 902, 58
Liao, K. 2019, ApJ, 885, 70
Liao, K., Shafieloo, A., Keeley, R. E., & Linder, E. V. 2020, ApJL, 895, L29
Planck Collaboration, Aghanim, N., Akrami, Y., et al. 2020, A&A, 641, A6
Poulin, V., Smith, T. L., Karwal, T., & Kamionkowski, M. 2019, PhRvL, 122, 221301
Rasmussen, C. E., & Williams, C. K. I. 2006, Gaussian Processes for Machine Learning (Cambridge, MA: MIT Press)
Riess, A. G., Casertano, S., Yuan, W., Macri, L. M., & Scolnic, D. 2019, ApJ, 876, 85
Ross, A. J., Samushia, L., Howlett, C., et al. 2015, MNRAS, 449, 835
Sahni, V., Shafieloo, A., & Starobinsky, A. A. 2008, PhRvD, 78, 103502
Scolnic, D. M., Jones, D. O., Rest, A., et al. 2018, ApJ, 859, 101
Shafieloo, A., Kim, A. G., & Linder, E. V. 2012, PhRvD, 85, 123530
Shafieloo, A., Kim, A. G., & Linder, E. V. 2013, PhRvD, 87, 023520
Wong, K. C., Suyu, S. H., Chen, G. C. F., et al. 2020, MNRAS, 498, 1420